

Surface shape and contact pressure evolution in two component surfaces: application to copper chemical mechanical polishing

W.G. Sawyer*

Department of Mechanical and Aerospace Engineering, University of Florida, Gainesville, FL 32611, USA

Received 10 March 2003; accepted 27 October 2003

Two defects that arise from the polishing process in integrated circuits technology are erosion and dishing. In this manuscript a generic numerical model that is capable of describing these defects from a mechanics perspective is presented. This numerical model formulates evolution of surface shape for an initially flat sample made up of two distinct materials with different wear rates under constant average polishing pressure. A two parameter elastic foundation model is used for contact pressure calculations. Qualitatively, the results compare favorably to published experimental data collected for copper chemical mechanical polishing. Although entirely mechanical, such modeling may perhaps provide insight into the mechanics of the surface defects and errors encountered during polishing.

KEY WORDS: wear, composites, chemical mechanical polishing

1. Introduction

As feature sizes continue to decrease in integrated circuits technology, defects arising from the polishing process, such as erosion and dishing, greatly impact final yield. Conventional copper chemical mechanical polishing uses polymeric pads with slurries of fine abrasives. The goal is to achieve a planar surface of copper and barrier oxide. Each of the phases has a unique resistance to material removal, and the resulting non-planar surfaces, shown in figure 1, are typical of defects resulting from this process.

In this manuscript a generic model for the surface evolution of a two component system under constant polishing load is developed. The approach follows coupled evolution approaches that have been successful at predicting shape evolution for 2-dimensional mechanical systems such as the scotch-yoke [1,2] and the eccentrically mounted circular cam [3,4], although it is applied here to a multi-component system under initially uniform contact pressure. The approach changes the surface shape after each cycle using a simple wear model, and uses the new surface shape to calculate tribological conditions for the subsequent cycle; these calculations proceed iteratively with both the shape and contact pressure evolving.

Over the past decade, efforts have been made to include wear within numerical and finite element methods. In the tribology literature, these models use an Archard's wear model for the incremental wear predic-

tions (Archard's wear model (1957) [5] and Preston's model (1927) [6], used in CMP, both have removal rate proportional to contact pressure to the first power). These problems are computationally intensive because of the iterative nature of the contact calculations, and researchers often try to extrapolate results to reduce the number of computation cycles. Extrapolation errors in such calculations were cursorily addressed by Dickrell *et al.* [4].

Pödra and Andersson [7] performed a finite element analysis for a conical spinning contact, a hemispherically tipped pin sliding against a plane [8], and a sliding sphere-on-flat and cylinder-on-flat configuration [9]. Results from these models were compared favorably to pin-on-disk experiments, analytical models, and numerical simulations, respectively. In the numerical simulation a Winkler model (elastic foundation) [10] was used to calculate contact pressures. These numerical predictions were in good agreement with the finite element analyses; this result is perhaps fortuitous given the planar nature of the evolving surface and uniform contact pressure predicted by both the finite element analysis and Winkler model. Winkler models for contact have also been used in coupled evolution solutions for spur gears [11] although the appropriateness of such a model to this contact problem is dubious.

In orthopaedic tribology the Winkler model and Archard's wear model were used in conjunction to estimate the wear of ultra-high-molecular-weight polyethylene tibial bearing components in total knee replacements [12]. Previously, Maxian *et al.* [13–15] used finite element analysis with coupled evolutions in shape

*E-mail: wgsawyer@ufl.edu

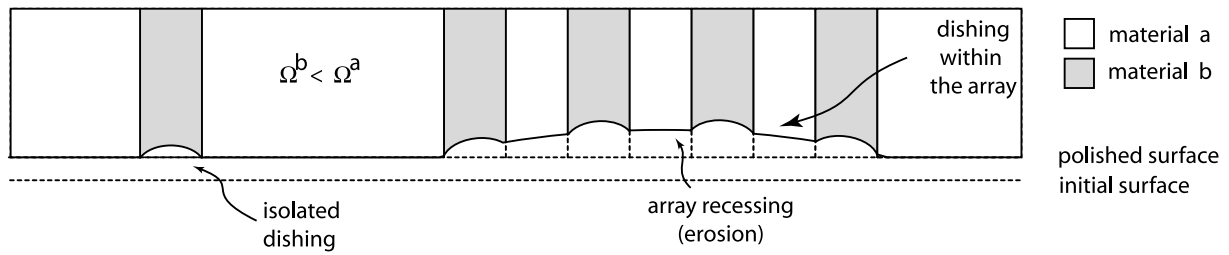


Figure 1. Schematic of the surface defects in multi-component polishing. While dishing generally refers to the recessing of an individual compartment, the recessing of arrays of such compartments is termed erosion.

and pressure for the polyethylene components in total hip replacements. Kurtz *et al.* [16] extended this work to include wear on both the articulating and backside of the polyethylene component.

Tugbawa *et al.* [17–21] and Park *et al.* [22] have done extensive experimental and theoretical work on the evolution of surface features in copper CMP. The numerical procedure suggested for modeling these defects in copper CMP is very similar to the coupled evolution processes discussed above. Unlike this previous work, which is specific to CMP processes, this manuscript sets up a more generic problem, and formulates the evolution of surface shape for an initially flat sample made up of two distinct materials with different wear rates. A two-parameter elastic foundation model is used for contact-pressure calculations. The problem addressed is motivated by the dishing and erosion seen in copper CMP and efforts to understand the mechanics of such surface evolution

in polishing, although the approach offered is not restricted to CMP and ignores chemical and fluid dynamic effects.

2. Modeling

The two-parameter elastic foundation model [23] is generally based on the pressure–displacement relationship given by equation (1), where p is the foundation reaction pressure, z is the deflection of the foundation, k_s is the first foundation parameter, and k_g is the second foundation parameter. The deflection of the pad under uniform applied pressure P_0 is given by equation (2). The problem description and some nomenclature are illustrated in figure 2.

$$p = k_s z - k_g \frac{d^2 z}{dx^2} \quad (1)$$

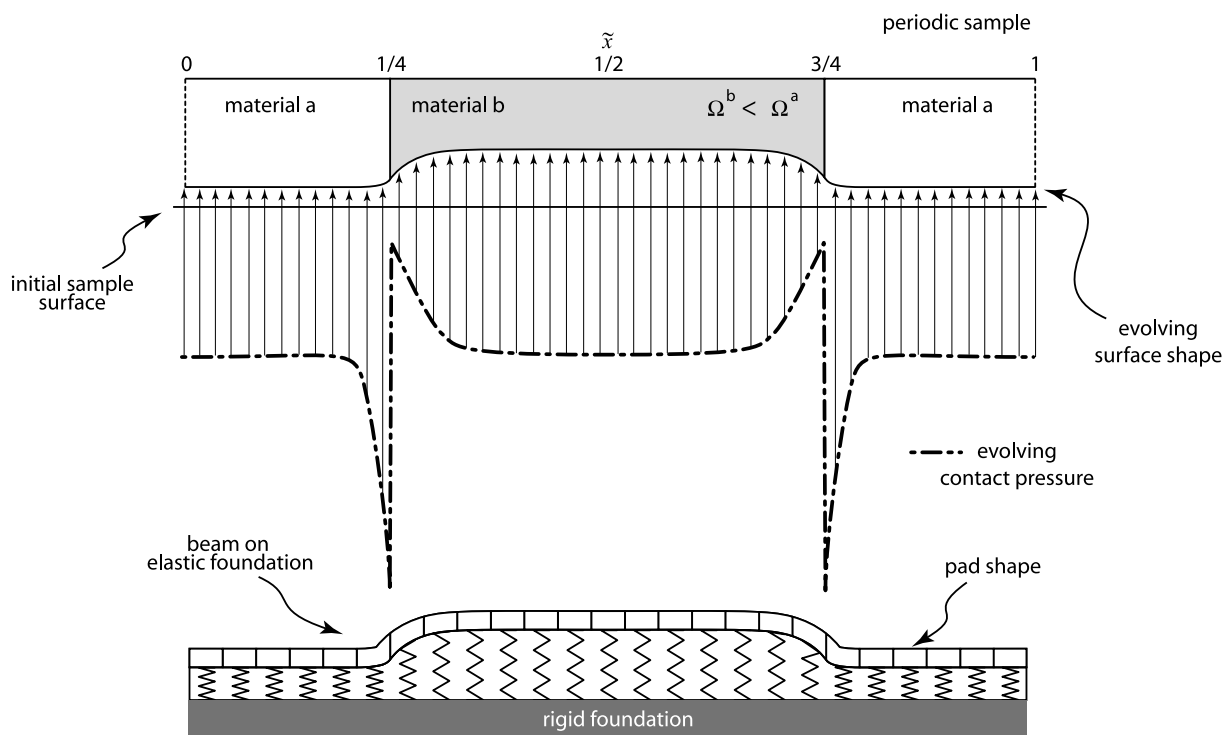


Figure 2. A schematic of the contact problem.

$$z_0 = \frac{P_0}{k_s} \quad (2)$$

The gross pad deflection in CMP is well estimated by the Winkler foundation model ($k_g = 0$), which is often used in modeling the CMP process due to the planar surfaces. However, because the Winkler model assumes no coupling between neighboring elements of the pad, which is the usefulness of the second parameter that is akin to a beam lying across the elastic foundation, at regions where the surface is not planar the Winkler model will under or over predict the contact pressure depending on the curvature direction. In this manuscript the second term is carried through in the analysis, as the manuscript aims to explore the mechanics behind the evolution in surface geometry from planar to non-planar.

The incremental depth of wear (Δh) at a particular location on the indenting solid is calculated using equation (3), where Δs is an incremental slip distance and Ω is the wear resistance of the material. Because the problem formulated assumes two materials on the sample, the superscripts a and b denote the material specific wear resistances (Ω^a is the material with greater wear resistance, and Ω^b the material with lower wear resistance). Wear models by Archard [5], Burwell and Strang [24], Holm [25], Preston [6], and Taylor [26] can all (with some algebra) be represented in the form of equation (3).

$$\Delta h = \frac{p\Delta s}{\Omega} \quad (3)$$

The iterative solution procedure is outline in figure 3. The coupled evolution of wear and contact pressure along the sample surface is studied here using an iterative numerical approach, where each differential surface element is assigned a specific wear resistance. And while single values of wear resistance were assumed in this study, the iterative solution methodology can easily accommodate pressure, speed, or time-dependent material-removal rate relationships.

The cumulative depth of wear after N simulation steps is found by summing all of the incremental depths of wear, as shown by equation (4), where the subscript (i) is used to denote a particular simulation step.

$$H = \sum_{i=1}^N \Delta h_i \quad (4)$$

3. Non-dimensionalization

In this section the dimensionless basic and working equations are developed, where the tilde (\sim) denotes a dimensionless variable. The non-dimensional surface

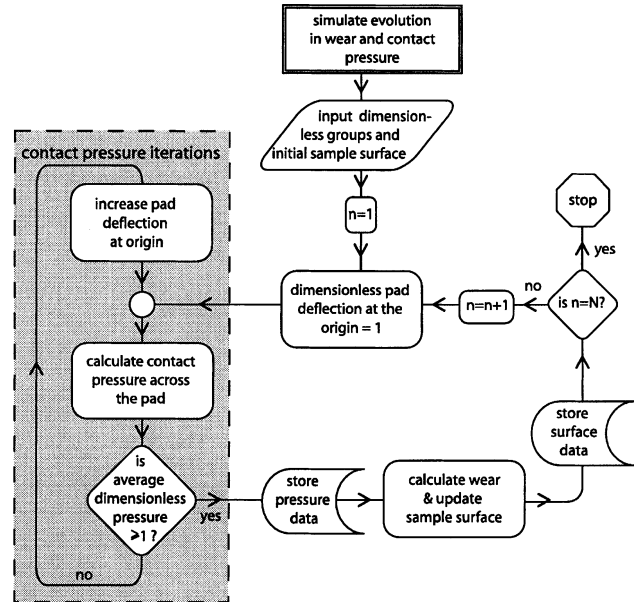


Figure 3. Flowchart of the numerical solution procedure.

coordinate, \tilde{x} , and pad deflection, \tilde{z} , are given by equations (5) and (6) respectively.

$$\tilde{x} = \frac{x}{l} \quad (5)$$

$$\tilde{z} = \frac{z}{z_0} = \frac{zk_s}{P_0} \quad (6)$$

Making the appropriate substitutions, the dimensionless pad pressure \tilde{p} is given by equation (7), where the dimensionless pad parameter $\tilde{\lambda}$ is described by equation (8).

$$\tilde{p} = \frac{p}{P_0} = \tilde{z} - \tilde{\lambda} \frac{d^2 \tilde{z}}{d\tilde{x}^2} \quad (7)$$

$$\tilde{\lambda} = \frac{k_g}{k_s l^2} \quad (8)$$

The individual wear resistances are normalized by the wear resistance of material a, which has the greater wear resistance. A dimensionless evolution parameter $\tilde{\beta}$, similar to a parameter termed “wear compliance” in a coupled evolution paper [3], is given by equation (11).

$$\tilde{\Omega}^a = 1 \quad (9)$$

$$\tilde{\Omega}^b = \frac{\Omega^b}{\Omega^a} \quad (10)$$

$$\tilde{\beta} = \frac{k_s \Delta s}{\Omega^b} \quad (11)$$

The incremental change in wear depth $\Delta\tilde{h}_i$ at a particular time (denoted by the subscript i) is given by the series of equations (12)–(14), where the superscript (a, b) should be read a or b .

$$\Delta\tilde{h}_i^{a,b} = \frac{\Delta h_i \Omega^b}{P_0 \Delta s} = \tilde{p}_i \frac{\tilde{\Omega}^b}{\tilde{\Omega}^{a,b}} \quad (12)$$

$$\Delta\tilde{h}_i^a = \tilde{p}_i \tilde{\Omega}^b \quad (13)$$

$$\Delta\tilde{h}_i^b = \tilde{p}_i \quad (14)$$

Due to the setup of the periodic surface description, the cumulative depth of wear at $\tilde{x} = 0$ is the lowest on the surface. The pressure at this location at any simulation step is denoted as $p_i|_0$ and the cumulative depth of wear at this location after N simulation steps is denoted as $H_N|_0$ and is given by equation (15). The depth of wear at other surface locations relative to the depth of wear at the $\tilde{x} = 0$ location is given by equation (16).

$$H_N|_0 = \sum_{i=1}^N \frac{p_i|_0 \Delta s}{\Omega^a} = \frac{\Delta s}{\Omega^a} \sum_{i=1}^N p_i|_0 \quad (15)$$

$$H' = H - H|_0 \quad (16)$$

The pad deflection z at various locations is a function of the pad deflection at the origin δ_0 and the surface elevations of the sample relative to this location. This is described by equation (17). Following the previously described dimensionless pad deflection, the deflection at the origin is normalized as shown by equation (18).

$$z = \delta_0 - H \quad (17)$$

$$\tilde{\delta}_0 = \frac{\delta_0}{z_0} \quad (18)$$

After performing the appropriate substitutions, the normalized pad deflection after N simulation iterations is given by equation (19), and is expressed more compactly for the elements of material a and b in equations (20) and (21), respectively.

$$\tilde{z}_N^{a,b} = \frac{z}{z_0} = \frac{(\delta_0 - H)}{z_0} = \tilde{\delta}_0 - \left(\frac{\tilde{\Omega}^b}{\tilde{\Omega}^{a,b}} \sum_{i=1}^N \tilde{p}_i - \tilde{\Omega}^b \sum_{i=1}^N \tilde{p}_i|_0 \right) \tilde{\beta} \quad (19)$$

$$\tilde{z}_N^a = \tilde{\delta}_0 - \left(\sum_{i=1}^N \tilde{p}_i - \sum_{i=1}^N \tilde{p}_i|_0 \right) \tilde{\Omega}^b \tilde{\beta} \quad (20)$$

$$\tilde{z}_N^b = \tilde{\delta}_0 - \left(\sum_{i=1}^N \tilde{p}_i - \tilde{\Omega}^b \sum_{i=1}^N \tilde{p}_i|_0 \right) \tilde{\beta} \quad (21)$$

4. Results and discussion

A numerical simulation was run under the following conditions: $\tilde{\lambda} = 0.1$, $\tilde{\beta} = 1.0 \times 10^{-4}$ and $\tilde{\Omega}^b = 0.2$. Figure 4 shows the evolution of the surface geometry and the contact pressure. The surface wear data is normalized as shown by equation (22).

$$\tilde{H}' = \frac{H - H|_0}{z_0} \quad (22)$$

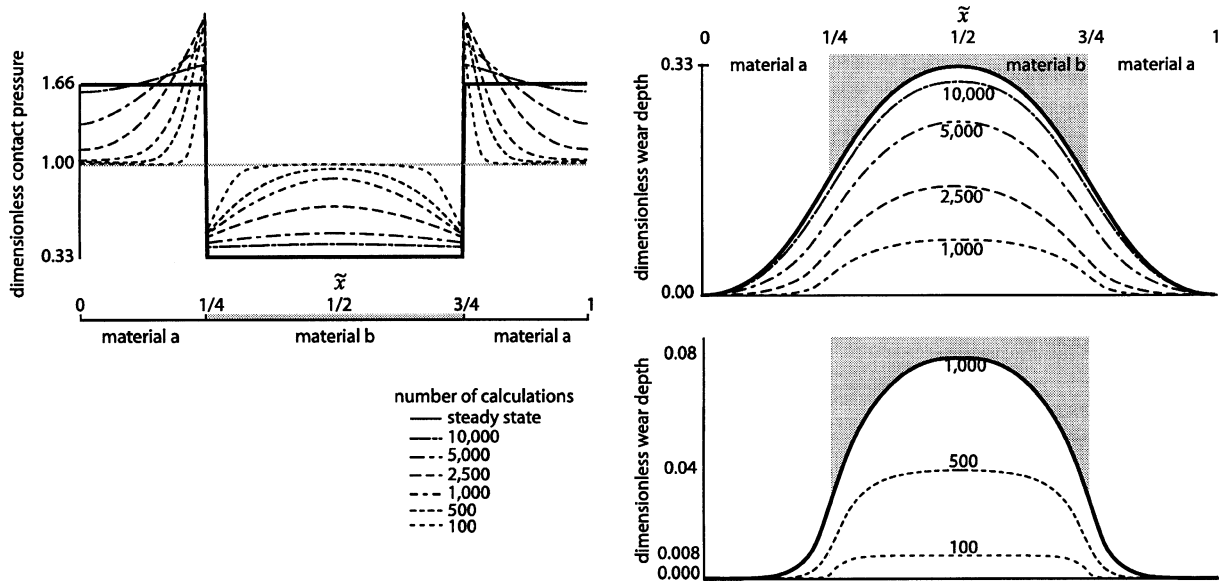


Figure 4. Results from numerical simulation ($\tilde{\lambda} = 0.1$, $\tilde{\beta} = 1.0 \times 10^{-4}$, and $\tilde{\Omega}^b = 0.2$) the evolution in contact pressure is shown to the left and evolution in surface geometry is on the right.

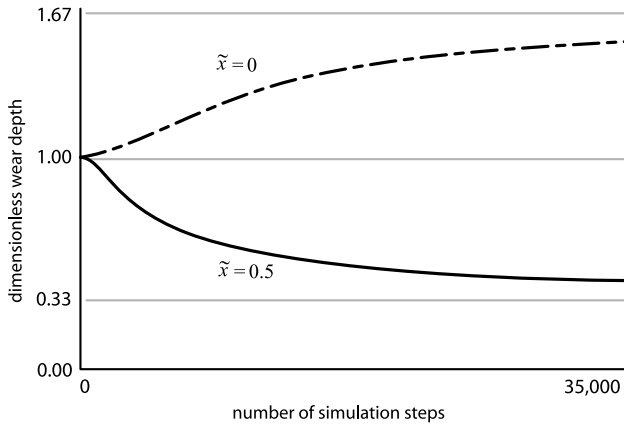


Figure 5. Results from numerical simulation ($\tilde{\lambda} = 0.1$, $\tilde{\beta} = 1.0 \times 10^{-4}$, and $\tilde{\Omega}^b = 0.2$) the evolution in normalized wear-depth for $\tilde{x} = 0$ and $\tilde{x} = 0.5$ is shown.

Figure 5 shows the progression of wear depth at the $\tilde{x} = 0$ location and $\tilde{x} = 0.5$ location, normalized as given in equations (23) and (24). This normalization process divides the wear at the origin location by the depth of wear that would be expected, assuming that the initial contact pressure does not evolve; rather, the pressure remains constant during the polishing process. For the $\tilde{x} = 0$ location all of these values are greater than unity, which indicates that the evolution of material removal and pressure at this location are increasing, conversely the $\tilde{x} = 0.5$ location has the opposite behavior suggesting the pressure at this location is decaying. Figure 6 shows the progression of normalized pressure at the $\tilde{x} = 0$ location and $\tilde{x} = 0.5$ location.

$$\tilde{H}_N|_0 = \frac{\sum_{i=1}^N \frac{p_i|_0 \Delta s}{\Omega^a}}{NP_0 \Delta s / \Omega^a} = \frac{1}{N} \sum_{i=1}^N \frac{p_i|_0}{P_0} \quad (23)$$

$$\tilde{H}_N|_{0.5} = \frac{\sum_{i=1}^N \frac{p_i|_{0.5} \Delta s}{\Omega^b}}{NP_0 \Delta s / \Omega^b} = \frac{1}{N} \sum_{i=1}^N \frac{p_i|_{0.5}}{P_0} \quad (24)$$

Because of the differential wear resistances the second-order derivatives are initially very large at the regions between the domains. These derivatives are handled numerically by fitting analytical functions through the neighboring points such that the derivatives are continuous; this is described in more detail in [4].

For these conditions, the dished geometry of the region with lower wear resistance is clearly evident. It is interesting to note the predictable and simple steady-state condition that shows two distinct regions of uniform pressure. The ratio of pressure borne by the region of lower wear resistance to the pressure

borne by the region of higher wear resistance is the same as the ratio of the wear resistances, which is described in equation (25). The average dimensionless contact pressure $\langle \tilde{p} \rangle$ follows a linear rule of mixtures as shown in equation (26), where $\tilde{\theta}$ is the dimensionless initial surface area fraction.

$$\frac{\tilde{p}_{\text{steady-state}}^b}{\tilde{p}_{\text{steady-state}}^a} = \frac{\Omega^b}{\Omega^a} \quad (25)$$

$$\langle \tilde{p} \rangle = \tilde{p}_{\text{steady-state}}^a \tilde{\theta}^a + \tilde{p}_{\text{steady-state}}^b \tilde{\theta}^b = 1 \quad (26)$$

The development of a steady-state profile requires that the pressures be constant on each of the regions. If otherwise, the removal of material will occur at different rates within a region, which is obviously not steady state. The ratio of the pressures is also expected because only when such a ratio of contact pressures is achieved will the rate of surface removal be equal at all locations along the sample. Equations (25) and (26) can be solved to give expressions for the steady-state non-dimensional pressure on each of the constituents; this is shown in equations (27) and (28) where the additional equation $\tilde{\theta}^a + \tilde{\theta}^b = 1$ is used during the simplification.

$$\tilde{p}_{\text{steady-state}}^a = \frac{1}{(\tilde{\theta}^a - \tilde{\theta}^a \tilde{\Omega}^b + \tilde{\Omega}^b)} \quad (27)$$

$$\tilde{p}_{\text{steady-state}}^b = \frac{\tilde{\Omega}^b}{(\tilde{\theta}^a - \tilde{\theta}^a \tilde{\Omega}^b + \tilde{\Omega}^b)} \quad (28)$$

Figure 6 shows the progression of contact pressure at $\tilde{x} = 0$ and $\tilde{x} = 0.5$ locations, which correspond to the location of minimum and maximum wear depth,

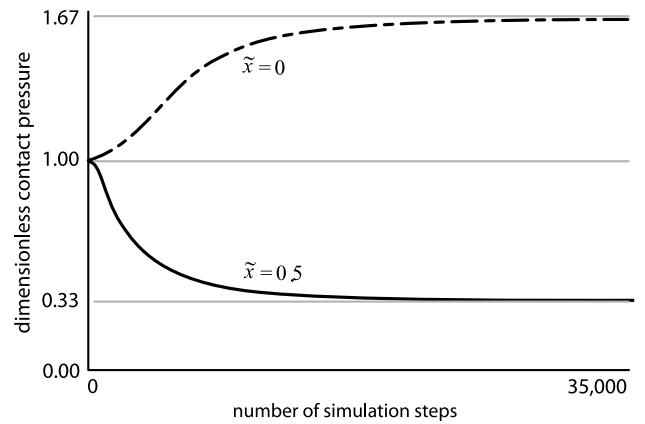


Figure 6. Results from numerical simulation ($\tilde{\lambda} = 0.1$, $\tilde{\beta} = 1.0 \times 10^{-4}$, and $\tilde{\Omega}^b = 0.2$) the evolution in contact pressure for $\tilde{x} = 0$ and $\tilde{x} = 0.5$ is shown.

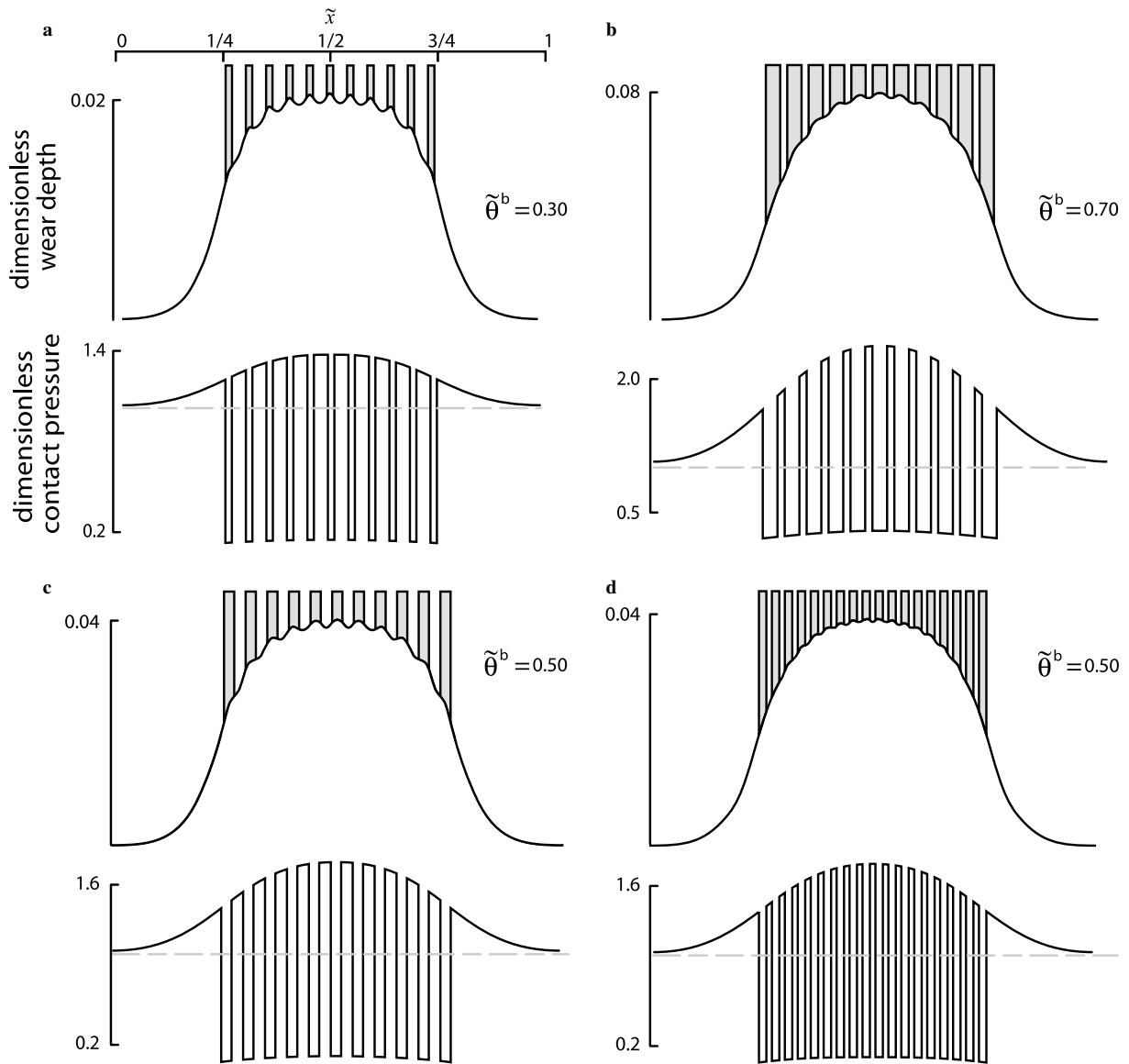


Figure 7. Results from numerical simulation ($\tilde{\lambda} = 0.1$, $\tilde{\beta} = 1.0 \times 10^{-4}$, and $\tilde{\Omega}^b = 0.1$) with constant line width after 5000 compute cycles, the noted area fractions are within the central pattern. (a) dimensionless line width 0.015 and dimensionless line spacing 0.035, (b) dimensionless line width 0.035 and dimensionless line spacing 0.015, (c) dimensionless line width 0.025 and dimensionless line spacing 0.025, and (d) dimensionless line width 0.015 and dimensionless line spacing 0.015.

respectively. A force balance requires the average non-dimensional pressure to be unity, $\langle \tilde{p} \rangle = 1$, which is described in equation (26) where $\tilde{\theta}^a$ and $\tilde{\theta}^b$ are the surface area fractions of material a and b respectively. In the isolated dishing problem formulation the surface area fractions are equal, $\tilde{\theta}^a = \tilde{\theta}^b = \frac{1}{2}$.

Pattern dependencies on erosion are investigated using the same model, by varying the number of evenly spaced regions of the material with lower wear resistance over the central area. Results from the numerical simulation $\tilde{\lambda} = 0.1$, $\tilde{\beta} = 1.0 \times 10^{-4}$, and $\tilde{\Omega}^b = 0.1$) with constant line width after 5000 compute cycles are shown in figure 7, the noted surface area fractions on the figure are within the central pattern. The simulation predicts qualitatively what is seen in

copper chemical mechanical polishing experiments. Namely, the recessing of the copper array (erosion) is very sensitive to the surface area fraction of the copper and not particularly sensitive to the line width of the copper. Supporting experimental data published by Tugbawa *et al.* [18] is plotted in figure 8. The steady-state pressure partitioning equations (26) and (27) suggest the origin of this pattern dependency. As the area fraction of less wear resistant material (b) increases within the central region the contact pressure borne by the more wear resistant material (a) increases, thus, causing more rapid evolution in wear within the region. The importance of the second term in the two-parameter elastic foundation model is clearly evident, as the model predicts the appearance of both dishing

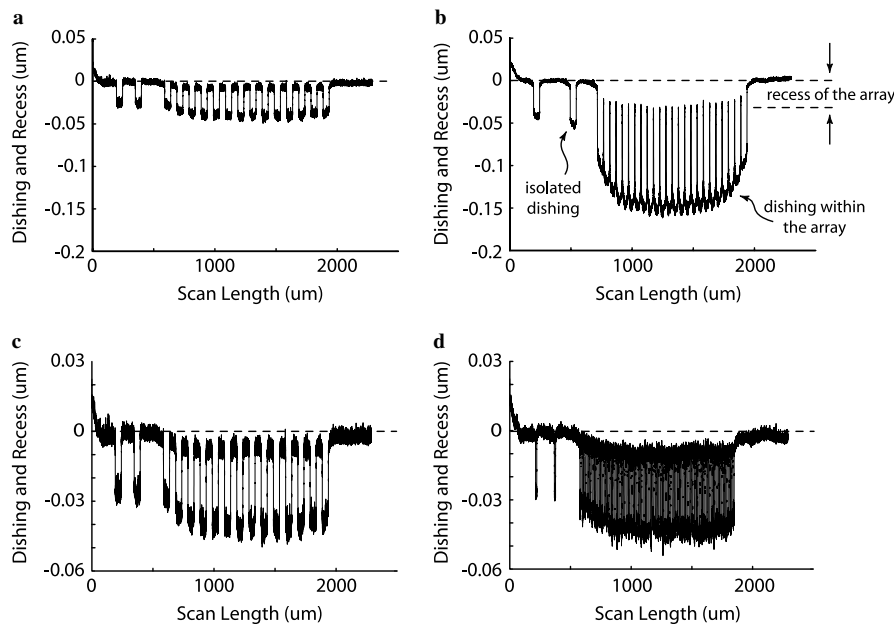


Figure 8. Experimental data from profilometer scans from Tugbawa *et al.* [18]. (a) copper line width $50\ \mu\text{m}$ and spacing $50\ \mu\text{m}$, (b) copper line width $50\ \mu\text{m}$ and spacing $1\ \mu\text{m}$, (c) copper line width $50\ \mu\text{m}$ and spacing $50\ \mu\text{m}$, and (d) copper line width $10\ \mu\text{m}$ and spacing $10\ \mu\text{m}$.
Note: the data shown here is plotted upside down from the convention used in this manuscript.

and erosion, while the Winkler model predicts only dishing.

5. Conclusion

The evolution of surface shape for an initially flat sample made up of two distinct materials with differing wear rates is formulated using a two parameter elastic foundation model for contact pressure calculations. Qualitatively, the results compare favorably to published experimental data collected for copper CMP and the trends seen in such data. Perhaps such modeling may provide insight to the mechanics of such surface defects and errors encountered during polishing.

References

- [1] T.A. Blanchet, *J. Tribol.* 119 (1997) 597.
- [2] W.G. Sawyer, K.I. Diaz, M.A. Hamilton and B. Micklos, *J. Tribol.* 125 (2003) 678.
- [3] W.G. Sawyer, *Lubr. Eng.* (2001) 31.
- [4] J.D. Dickrell, D.B. Dooner and W.G. Sawyer, *J. Tribol.* 125 (2003) 187.
- [5] J.F. Archard, *J. Appl. Phys.* 24 (1953) 981.
- [6] F.W. Preston, *J. Soc. Glass Technol.* 11 (1927) 214.
- [7] P. Pödra and S. Andersson, *Wear* 224 (1999) 13.
- [8] P. Pödra and S. Andersson, *Tribol. Int.* 32 (1999) 71.
- [9] P. Pödra and S. Andersson, *Wear* 207 (1997) 79.
- [10] E. Winkler, *The Science of Elasticity and Firmness* (Prag: Dominicus, 1867) [Die Lehre von der elasticitaet und festigkeit, in German].
- [11] A. Flodin and S. Andersson, *Wear* 207 (1997) 16.
- [12] B.J. Fregly, W.G. Sawyer, M.K. Harman and S.A. Banks, *J. Biomech.*, in Press.
- [13] T.A. Maxian, T.D. Brown, D.R. Pedersen and J.J. Callaghan, *Am. Soc. Mech. Eng. Bioeng. Div. (Publ.) BED* 31 (1995) 237.
- [14] T.A. Maxian, T.D. Brown, D.R. Pedersen and J.J. Callaghan, *J. Orthop. Res.* 14 (1996) 668.
- [15] T.A. Maxian, T.D. Brown, D.R. Pedersen and J.J. Callaghan, *J. Biomech.* 29 (1996) 687.
- [16] S.M. Kurtz, J.A. Ochoa, C.B. Hovey and C.V. White, *J. Biomech.* 32 (1999) 967.
- [17] T. Tugbawa, T. Park, D. Boning, T. Pan, P. Li, S. Hymes, T. Brown and L. Camilletti, *CMP Symposium, Electrochemical Society Meeting, Honolulu, HA* (1999).
- [18] T. Tugbawa, T. Park, B. Lee, D. Boning, P. Lefevre and J. Nguyen, *VLSI Multilevel Interconnect Conference, Santa Clara, CA* (2001).
- [19] T. Tugbawa, T. Park, B. Lee, D. Boning, P. Lefevre and L. Camilletti, *Materials Research Society (MRS) Spring Meeting, San Francisco, CA* (2001).
- [20] T. Tugbawa, T. Park, D. Boning, L. Camilletti, M. Brongo and P. Lefevre, *Chemical Mechanical Polish for ULSI Multilevel Interconnection Conference, Santa Clara* (2001) 65.
- [21] T. Tugbawa, T. Park and D. Boning, *International Interconnect Technology Conference, San Francisco, CA* (2002).
- [22] T. Park, T. Tugbawa and D. Boning, *Chemical Mechanical Polish for ULSI Multilevel Interconnection Conference CMP-MIC Santa Clara* (2000) 196.
- [23] P.L. Pasternak, *On a New Method of Analysis of an Elastic Foundation by Means of Two-Constants* (Moscow, USSR: Gosudarstvennoe Izdatelstvo Literaturi po Stroitelstvu i Arkhitekture, 1954) [in Russian].
- [24] J.T. Burwell and C.D. Strang, *J. Appl. Phys.* 23 (1952) 18.
- [25] R. Holm, *Electrical Contacts* (Springer-Verlag, New York, 1946).
- [26] F.W. Taylor, *Trans. ASME* 28 (1906) 31.